Backgro nd

DNA methylation is central to establishing and maintaining tissue-specific gene expression, and an important contributing factor to oncogenesis. We recently demonstrated that pervasive and ablating conditions of tumor hypoxia drive DNA methylation of tumor suppressor genes by reducing the activity of TET DNA demethylases [1]. An outstanding question is, however, if and how DNA methylation in turn also influences the response of tumors to (acute) hypoxia. Indeed, recent evidence suggests that, contrary to traditional concepts, DNA methylation generally does not directly impede transcription factor (TF) binding, but rather acts indirectly by synergizing with other epigenetic marks [2].

The hypoxia response is canonically executed by HIFs, which are heterodimeric TF complexes composed of an O_2-labile α-subunit (HIF1α, HIF2α or HIF3α) and a stable β-subunit (HIF1β). The constitutively expressed HIFα subunits are directly targeted for proteasomal degradation under normal oxygen tension (normoxia), but stabilized under limiting oxygen conditions (hypoxia), when they translocate to the nucleus to induce expression of hypoxia-responsive genes. This induction of hypoxia-responsive genes occurs rapidly, often within minutes following hypoxia [3

Results

DNA methylation of HRE sites anti-correlates with HIF binding

To investigate the role of DNA methylation in HIF binding, we stabilized HIFs in MCF7 breast cancer cells by culturing them under acute hypoxia (0.5% O_2 for 16 h; Additional file 1: Fig. S1a and S2, and "Methods"), conditions that are insufficient to drive hypoxia-induced hypermethylation [1]. We next performed chromatin-immunoprecipitation coupled to high-throughput sequencing (ChIP-seq) for HIF1β, which is the obligate dimerization partner of HIF1α, HIF2α, and HIF3α. Model-based analysis for ChIP-seq (MACS) [16] revealed 7153 HIF1β binding peaks (Fig. 1a, Table S1). These were high-quality, bona fide HIF binding regions: they were 4.6-fold enriched for the HRE motif (RCGTG), enriched near genes involved in the hypoxia response, > 90% overlapping with peaks identified in another HIF1β ChIP-seq dataset on MCF7 cells and reproducibly detected in independent repeats (Additional file 1: Fig. S1b-d).

To assess methylation in these 7153 HIF1β binding peaks, we performed target enrichment-based bisulfite sequencing (BS-seq) on DNA extracted from normoxic MCF7 cells, in which HIF is inactive, obtaining > 40× coverage for ~ 86% of the HIF1β binding peaks identified by ChIP-seq. The methylation level at these peaks was invariably low (4.95 ± 0.15%) compared to average CpG methylation levels detected in the genome (61.6 ± 0.07%, Wilcoxon test $< 2.2^{-16}$, Fig. 1b). Results were confirmed using another whole-genome BS-seq dataset (Fig. 1a) [18]. Also when quantifying methylation across all RCGTG motifs, including those located outside of HIF1β binding peaks, the inverse correlation between DNA methylation and HIF binding was confirmed (Fig. 1c). As BS-seq does not discriminate between 5-methyl (5mC) and 5-hydroxymethylcytosine [19], we confirmed by DNA immunoprecipitation with an antibody recognizing only 5mC (5mC-DIP-seq) that HIF1β binding peaks were six fold depleted in 5mC-DIP-seq reads (Fig. 1a). Moreover, methylation analysis of normoxic *1* -knockout MCF7 cells [20] revealed identical methylation patterns (Additional file 1: Fig. S1e-g), indicating that the unmethylated state of HIF1β

and unique for an individual cell line at 7140 sites (437, 1193, and 5510 unique sites, respectively for RCC4, MCF7, and SK-MEL-28) (Fig. 1d, Additional file 1: Fig. S1k-l). Crucially, when assessing DNA methylation both under normoxia and under acute hypoxia, HIF1β binding peaks unique to individual cell lines were unmethylated in cells where the binding site was active, while active HIF1β binding peaks shared between all cell lines were unmethylated in all cell lines (Fig. 1e, f, Additional file 1: Fig. S1m-n). This strict correlation suggests that DNA methylation underlies the cell-type-specific response to hypoxia. Differences in DNA methylation and concomitant HIF binding also appeared functional, as transcriptome profiling under normoxic and hypoxiconditionas reie

HIF1β binding peaks [12]. This was confirmed in linear regression analyses assessing how each mark individually predicts HIF1β binding in MCF7 cells. DNA methylation (^{2}

differences in the chromatin profiles of HIF1α- and HIF2α-bound regions: HIF1α binding sites showed 1.37-fold higher average levels of the promoter mark H3K4me3, whereas levels of the enhancer mark H3K4me1 were 0.75-fold lower at HIF1α binding sites than at HIF2α

for an unmethylated than methylated RCGTG motif, thus confirming that methylation directly repels binding of HIF1α-HIF1β and HIF2α-HIF1β heterodimers (Fig. 2e, f). Indeed, leveraging the crystal structure of the HIF1α-HIF1β and the HIF2α-HIF1β complexes bound to DNA [25], revealed that both cytosines in the CpG dinucleotide of the

Waals radii and would be poised to cause severe steric clashes with these two functionally important arginine residues in HIF1α or HIF2α (Fig. 2h).

DNA demethylation enables ectopic HIF binding

Next, we investigated which parts of the genome are protected from HIF binding by DNA methylation. For this, we compared HIF1β binding in hypoxic wild-type murine ESCs versus ESCs deficient for DNA methyltransferases (-TKOs), which lack DNA methylation [27], using HIF1β ChIP-seq (= 4 replicates for each; for data quality assessment see Additional file 1: Fig. S5). This revealed a marked increase in the number of HIF1β binding peaks, from 7875 in wild-type to 9806 in -TKO ESCs (Fig. 3a). Whole-genome BS-seq further revealed that, while shared binding peaks were unmethylated in both cell lines, -TKO-specific HIF1β binding peaks had high methylation levels in wild-type ESCs (Fig. 3b).

All shared binding peaks were associated with a similar enrichment of the RCGTG motif (Fig. 3c), as well as with genes that were induced upon hypoxia (Fig. 3d). However, -TKO-specific sites were more often distal to annotated transcription start sites (TSS) or regions of open chromatin, and more frequently in repressed chromatin regions of wild-type ESCs (Fig. 3e–g). Gene ontology analysis moreover failed to identify enrichment of hypoxia-related processes for -TKO-specific binding peaks, in contrast to shared peaks (Fig. 3h). Thus, the majority of these -TKO-specific binding peaks represents ectopic binding events.

DNA methylation represses hypoxia-induced expression of retrotransposons

Indeed, a substantial fraction of novel

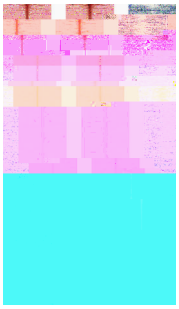

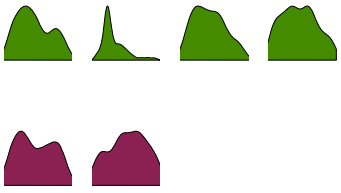

binding peaks were often distal to TSSs, and binding at LTRs was enriched over a randomization of HIF1β binding site positions (Fig. 4

CRyptic Elements' Differential Expression by de Novo Transcriptome Reconstruction (CREDENToR). CREDENToR first performs a de novo transcriptome assembly to define cryptic transcripts and then assigns uniquely mapping reads to them to quantify their expression. The cryptic transcripts detected by CREDENToR are poorly conserved, often unspliced transcripts, shorter than lincRNAs but expressed at similar levels (see "Methods" and Additional file 1: Fig. S7b-g for benchmarking).

CREDENToR identified that out of 1389 differentially expressed cryptic transcripts (1% FDR), 67% were upregulated by hypoxia (Additional file 1: Fig. S6k). As expected, focusing on HIF-bound cryptic transcripts revealed an even stronger enrichment, with 82% and 91% (respectively, at 1% and 0.001% FDR) differentially expressed transcripts being upregulated following hypoxia (Fig. 4e). HIF binding was enriched at the promoter of hypoxia-induced cryptic transcripts, but far less in those induced by aza (Additional file 1: Fig. S6l). Interestingly, significant fractions of cryptic transcripts contained palindromic repeats, or overlapped with other transcripts in the reverse orientation, and could thus produce double-stranded (ds) RNA. HIF-bound cryptic transcripts were twice as likely to generate such dsRNAs (Fig. 4f). Together, this suggests HIF binding

Overall, these observations support a model wherein hypoxia-induced cryptic tran-

breast cancer model was identified as low-immunogenic. Indeed, 4T1 tumors exhibited a low TMB, cytolytic activity, number of $CD8^+$ T cells and expression of immune checkpoints (*1*, *1*) compared to other models (Additional file 1: Fig. S9a). In line with 4T1 grafts being low-immunogenic tumors, anti-PD1 treatment failed to affect their growth (– 8%, = 0.397), while significantly reducing growth of high-immunogenic tumors, as described previously [41, 42] (Additional file 1: Fig. S9b). Im-

fold change *vs* vehicle

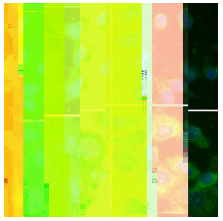

effect; = 0.021; Fig. 6j). The differential effect of aza in 4T1 $^{\textit{1}}$-KO versus 4T1 $^{\textit{1}}$-scr grafts was also highly significant in an interaction analysis (< 0.0001). Moreover, while the number of activated T cells increased in 4T1 $^{\textit{1}}$-scr grafts following aza, 4T1 $^{\textit{1}}$-KO

containing a permissive chromatin structure [15, 24]. Importantly, binding specificities for HIF1α versus HIF2α are independent of DNA methylation, but appear to be influ-

in a HIF-dependent manner. By showing that low-immunogenic, hypoxic tumors can be rendered immunogenic through DNA methylation inhibitors, we thus highlight a novel treatment strategy for tumors otherwise refractory to immunotherapies.

Methods

Materials

All materials were molecular biology grade. Unless noted otherwise, all were from Sigma (Diegem, Belgium).

Cell lines

MCF7, RCC4, SK-MEL-28, A549, 4T1, MC38, and CT26 cell lines were obtained from the American Type Culture Collection, and their identity was not further authenticated. None of these cell lines are listed in the database of commonly misidentified cell lines maintained by ICLAC. MCF7 *1* -knockout cells were previously described [20]. MCF7, RCC4, A549, MC38, and 4T1 cells were cultured at 37 °C in Dulbecco's modified Eagle's medium (DMEM) with 10% fetal bovine serum (FBS), 5 mL of 100 U/mL Penicillin-Streptomycin (Pen-Strep, Life Technologies), and 5 mL of L-glutamine 200 mM. SK-MEL-28 and CT26 cell lines were cultured at 37 °C in Roswell Park Memorial Institute 1640 Medium (RPMI) with 10% FBS 1% Pen-Strep and 1% L-glutamine.

Murine embryonic stem cells (mESCs) that were triple-knockout for *1*, , and (-TKO) and triple-knockout for *1*, *2*, and (-TKO) and their appropriate wild-type (WT) control mESCs were obtained from Dr. Masaki Okano and Dr. Guoliang Xu respectively [57, 58]. mESCs that were knockout for *1* (*1* - *)* and their WT control mESCs were previously described [21]. -TKO, -TKO, -WT, *1* -WT, and *1* -KO mESCs were cultured feeder-free in fibroblast-conditioned medium (DMEM with 4500 mg /L glucose, 2 mM L-glutamine, 1 mM sodium pyruvate, 15% FBS, 1% Pen-Strep, 0.1 mM of non-essential amino acids, 0.1 mM β-mercaptoethanol) on 0.1% gelatine-coated plates. mESCs from the 159 background used for the recombinase-mediated cassette exchange reaction were kindly provided by Prof. Dirk Schubeler (Friedrich Miescher Institute for Biomedical Research, Basel, Switzerland) and grown in ESC medium (DMEM with 4500 mg /L glucose, 2 mM L-glutamine, 1 mM sodium pyruvate, 15% FBS, 1%

expression level. Where indicated, cells were pre-treated with 5-aza-2′-deoxycytidine (aza, 1 μM) for 3 days by adding the required volume to fresh culture medium. Equal volumes of the carrier (DMSO) were used as control. This was followed by another day of exposure to aza in hypoxia or normoxia, bringing the total aza exposure time for experiments to 4 days. Then, 2 mM of DMOG (dimethyloxalylglycine, Sigma) was added to culture

the whole genome for RCGTG motifs using the regular expression search tool dreg
(

the following mix: 5 µL of 10× NEBuffer 2, 1.5 µL of 10 mM dNTP mix (10 mM dATP, dCTP, dGTP, dUTP, Sigma), 0.1 µL of RNaseH (10 U/µL, Ambion), 2.5 µL of DNA Polymerase I Klenov (10 U/µL, NEB), and water until 50 µL. The eluted cDNA was incubated for 30 min at 16 °C, purified by Agencourt AMPure XP, and eluted in 30 µL of dA-Tailing mix (2 µL of Klenow Fragment, 3 µL of 10× NEBNext dA-Tailing Reaction

the merged transcription annotations were assigned as cryptic transcripts when any of their exons overlapped with a retrotransposon repeat annotation (LTR, LINE, or SINE, based on RepeatMasker annotation from UCSC). If a transcript overlapped with > 1 annotated repeat, the retrotransposon with the highest overlap was assigned to this cryptic transcript.

For the analysis of MCF7 data, the assembled annotations from all experimental conditions involving MCF7 cells assessed in vitro were merged before read counting. For the analysis of 4T1 data, the assembled annotations from in vitro and in vivo samples were merged together. Cryptic transcripts were considered to be HIF-associated if a HIF binding summit was detected within the transcript promoter (i.e., 2000 bp upstream and 500 bp downstream of the transcription start site). Per set of experiments (24 samples), we

25 °C at 20% LED power and medium MST power. Data was normalized to % fraction bound, and the values for the equilibrium dissociation constant ($_D$) were calculated by fitting the curves in GraphPad Prism 7.

Generation of mESCs containing a methylated or unmethylated HIF binding region

A DNA fragment (human chr16:30,065,212-30,065,711) containing five CGTG motives was selected based on high HIF1β ChIP-enrichment in MCF7, RCC4, and SK-MEL-28 cells. Oligonucleotides were designed to amplify the target region (AGGTGCAATT GTTCCTCCGCCTCCCTTAC and AAGGGCAATTGCCGAGCTTTTTCCTTTACGA) and used for PCR amplification of the target region using the Q5® Hot Start High-Fidelity 2× Master Mix (NEB), followed by evaluation of the PCR products by gel electrophoresis and purification with the Qiaquick PCR purification kit (28104, Qiagen). These PCR primers were evaluated for specificity in human (MCF7, RCC4, SK-MEL-28) but not in mouse genomic DNA, while MfeI restriction sites were added to the ends of the primer pairs. The purified amplicon was digested with MfeI and cloned into the L1-poly-L1 plas-mid (provided by P1(%)-3505TL17.5(ma)13.1(n)-362((M)16.8(CF)11.1c5TL9.7999CFHSFi

specific primers for the cloned locus (oligonucleotides TCGTTTCCGACTTTTCCATC and CAGCCAGAATGTTGGCAAT) and an independent murine genomic region for background quantification (oligonucleotides CACTTGCTGAATAATTGGGTGT and CTGTTGTCCAGTTTTCTTCACG). Enrichment was calculated as fold enrichment over background.

the hypoxia metagene signature (, , , *1*, *2* *1*, *1*, *1*, , , *1*, *1*, , , , and) [37]. In each case, the top 2 subclusters identified were annotated as normoxic and hypoxic.

To test the interaction between hypoxia and DNA methylation, we assessed read counts for cryptic transcripts in two negative-binominal generalized linear models with both oxygenation (hypoxic and normoxic; encoded as 0 and 1) and methylation (low and high methylation; encoded as 0 or 1), with or without an interaction term. Both models were compared to each other using DESeq. A positive interaction coefficient represents a cooperative enhancement of cryptic transcript expression in low-methylation, hypoxic tumors. To further enrich for tumors that are prone to respond to checkpoint immunotherapy, we stratified all tumor types into high *1* mRNA expressing and low *1* mRNA expressing tumors, and into tumors with a high or low tumor mutation burden (TMB). Stratification was done on the third decile in both cases. TMB was estimated based on the number of substitutions identified by TCGA in each tumor sample. All substitutions were considered, except for those also present in non-malignant samples (i.e., exclusion of germline variants) or those clustering within and across different samples (and therefore most likely representing sequencing or mapping errors).

Single-cell analysis

A transformation mix containing viral particles, TE, $CaCl_2$, H_2

anti-CD8a 1:300, secondary antibody goat anti-rat (MP-7444, Vector) and opal 690

S pplementar information

Supplementary information accompanies this paper at https://doi.org/10.1186/s13059-020-02087-z.

Additional file 1: Fig. S1. HIF1β peaks in MCF7 cells under 0.5% O2. **Fig. S2.** Expression of hypoxia genes and cancer testis antigens. **Fig. S3.** Cell-type-specific HIF1β binding. **Fig. S4.** DNA methylation directly repels HIF1β binding. **Fig. S5.** Quality control of the ChIP-seq replicates. **Fig. S6.** HIF binds retrotransposons in demethylated genomes. **Fig. S7.** Examples of cryptic transcripts upregulated by HIF1β. **Fig. S8.** Cryptic transcript expression in TCGA tumors. **Fig. S9.** Aza treatment increases immunogenicity.

Additional file 2: Table S1. HIF1β binding peaks detected using MACS at $P < 10^{-15}$ in MCF7 cell line.

Additional file 3: Table S2. HIF1β binding peaks detected using MACS at $P < 10^{-15}$ across RCC4, MCF7 and SK-MEL-28 cell lines. For each cell line, HIF1β binding was annotated as 'present' if the peak area showed > 4-fold enrichment over the local read depth, and as 'absent' if it showed < 2.5-fold enrichment; intermediate enrichment scores were annotated as 'unclassified'.

Additional file 4: Table S3. Cryptic transcript promoter DNA methylation and expression levels. Shown are results from an analysis of combined single-cell methylome-and-transcriptome sequencing of colorectal cancer cells, as generated by Bian and colleagues [38].

Additional file 5. Review history.

Acknowledgements

We thank Masaki Okano and Guoliang Xu for murine Dnmt-TKO and Tet-TKO ESCs and the corresponding matching WT ESCs.

Review history

The review history is available as Additional file 5.

Peer review information

Anahita Bishop was the primary editor of this article and managed its editorial process and peer review in collaboration with the rest of the editorial team.

Authors'

Competing interests
The authors declare that they have no competing interests.

Author details
[1]Center for Cancer Biology, VIB, 3000 Leuven, Belgium. [2]Laboratory of Translational Genetics, Department of Human Genetics, KU Leuven, 3000 Leuven, Belgium. [3]Epigenetics Programme, Babraham Institute, Cambridge CB22 3AT, UK. [4]The Old Schools, University of Cambridge, Trinity Lane Cambridge CB2 1TN, UK.

24. Wu X, Zhang Y. TET-mediated active DNA demethylation: mechanism, function and beyond. Nat Rev Genet. 2017;18:517.
25. Wu D, Potluri N, Lu J, Kim Y, Rastinejad F. Structural integration in hypoxia-inducible factors. Nature. 2015;524:303–8.
26. Mariani CJ, Vasanthakumar A, Madzo J, Yesilkanal A, Bhagat T, Yu Y, Bhattacharyya S, Wenger RH, Cohn SL, Nanduri J, et al. TET1-mediated hydroxymethylation facilitates hypoxic gene induction in neuroblastoma. Cell Rep. 2014;7:1343–52.
27. Tsumura A, Hayakawa T, Kumaki Y, Takebayashi S, Sakaue M, Matsuoka C, Shimotohno K, Ishikawa F, Li E, Ueda HR, et al. Maintenance of self-renewal ability of mouse embryonic stem cells in the absence of DNA methyltransferases Dnmt1, Dnmt3a and Dnmt3b. Genes Cells. 2006;11:805–14.
28. Beyrouthy MJ, Garner KM, Hever MP, Freemantle SJ, Eastman A, Dmitrovsky E, Spinella MJ. High DNA methyltransferase 3B expression mediates 5-aza-deoxycytidine hypersensitivity in testicular germ cell tumors. Cancer Res. 2009;69:9360–6.
29. Criscione SW, Zhang Y, Thompson W, Sedivy JM, Neretti N. Transcriptional landscape of repetitive elements in normal and cancer human cells. BMC Genomics. 2014;15:583.
30. Yang WR, Ardeljan D, Pacyna CN, Payer LM, Burns KH. SQuIRE reveals locus-specific regulation of interspersed repeat expression. Nucleic Acids Res. 2019;47(5):e27.
31. Elvidge GP, Glenny L, Appelhoff RJ, Ratcliffe PJ, Ragoussis J, Gleadle JM. Concordant regulation of gene expression by hypoxia and 2-oxoglutarate-dependent dioxygenase inhibition the role of HIF-1α, HIF-2α, and other pathways. J Biol Chem. 2006;281:15215–26.
32. Blank CU, Haanen JB, Ribas A, Schumacher TN. CANCER IMMUNOLOGY. The "cancer immunogram". Science. 2016;352:658–60.
33. Chiappinelli KB, Strissel PL, Desrichard A, Li H, Henke C, Akman B, Hein A, Rote NS, Cope LM, Snyder A, et al. Inhibiting DNA methylation causes an interferon response in cancer via dsRNA including endogenous retroviruses. Cell. 2015;162:974–86.
34. Zitvogel L, Galluzzi L, Kepp O, Smyth MJ, Kroemer G. Type I interferons in anticancer immunity. Nat Rev Immunol. 2015;15:405–14.
35. Leruste A, Tosello J, Ramos RN, Tauziède-Espariat A, Brohard S, Han Z-Y, Beccaria K, Andrianteranagna M, Caudana P, Nikolic J. Clonally expanded T cells reveal immunogenicity of rhabdoid tumors. Cancer Cell. 2019;36(6):597-612.e8.
36. Rooney MS, Shukla SA, Wu CJ, Getz G, Hacohen N. Molecular and genetic properties of tumors associated with local immune cytolytic activity. Cell. 2015;160:48–61.
37. Buffa FM, Harris AL, West CM, Miller CJ. Large meta-analysis of multiple cancers reveals a common, compact and highly prognostic hypoxia metagene. Br J Cancer. 2010;102:428–35.